Event-by-event generation of electromagnetic fields in heavy-ion collisions

Wei-Tian Deng[1,*] and Xu-Guang Huang[1,2,†]

[1]*Frankfurt Institute for Advanced Studies, D-60438 Frankfurt am Main, Germany*

[2]*Institut für Theoretische Physik, J. W. Goethe-Universität, D-60438 Frankfurt am Main, Germany*

(Received 25 January 2012; revised manuscript received 22 February 2012; published 5 April 2012)

We compute the electromagnetic fields generated in heavy-ion collisions by using the HIJING model. Although after averaging over many events only the magnetic field perpendicular to the reaction plane is sizable, we find very strong electric and magnetic fields both parallel and perpendicular to the reaction plane on the event-by-event basis. We study the time evolution and the spatial distribution of these fields. In particular, the electromagnetic response of the quark-gluon plasma can give nontrivial evolution of the electromagnetic fields. The implications of the strong electromagnetic fields on the hadronic observables are also discussed.

DOI: 10.1103/PhysRevC.85.044907 PACS number(s): 25.75.Ag, 24.10.Jv, 24.10.Lx

I. INTRODUCTION

Relativistic heavy-ion collisions provide us the methods to create and explore strongly interacting matter at high energy densities where the deconfined quark-gluon plasma (QGP) is expected to form. The properties of matter governed by quantum chromodynamics (QCD) have been studied at the Relativistic Heavy Ion Collider (RHIC) at Brookhaven National Laboratory (BNL) and at the Large Hadron Collider (LHC) at CERN. Measurements performed at RHIC in Au + Au collisions at center-of-mass energy $\sqrt{s} = 200$ GeV per nucleon pair and at LHC in Pb Pb collisions at center-of-mass energy $\sqrt{s} = 2.76$ TeV per nucleon pair have revealed several unusual properties of this hot, dense matter (e.g., its very low shear viscosity [1,2], and its high opacity for energetic jets [3–6]).

Due to the fast, oppositely directed motion of two colliding ions, off-central heavy-ion collisions can create strong transient magnetic fields [7]. As estimated by Kharzeev, McLerran, and Warringa [8], the magnetic fields generated in off-central Au + Au collisions at RHIC can reach $eB \sim m_\pi^2 \sim 10^{18}$ G, which is 10^{13} times larger than the strongest man-made steady magnetic field in the laboratory. The magnetic field generated at LHC energy can be 10 times larger than that at RHIC [9]. Thus, heavy-ion collisions provide a unique terrestrial environment to study QCD in strong magnetic fields. It has been shown that a strong magnetic field can convert topological charge fluctuations in the QCD vacuum into global electric charge separation with respect to the reaction plane [8,10,11]. This so-called chiral magnetic effect may serve as a sign of the local P and CP violation of QCD. Experimentally, the STAR [12,13], PHENIX [14], and ALICE [15] Collaborations have reported the measurements of the two-particle correlations of charged particles with respect to the reaction plane, which are qualitatively consistent with the chiral magnetic effect, although there are still some debates [16–20].

Besides the chiral magnetic effect, there can be other effects caused by the strong magnetic fields including the catalysis of chiral symmetry breaking [21], the possible splitting of chiral and deconfinement phase transitions [22], the spontaneous electromagnetic superconductivity of QCD vacuum [23,24], the possible enhancement of elliptic flow of charged particles [25,26], the energy loss due to the synchrotron radiation of quarks [27], the emergence of anisotropic viscosities [26,28,29], the induction of the electric quadrupole moment of the QGP [30], etc.

The key quantity of all these effects are the strength of the magnetic fields. Most of the previous works estimated the magnetic-field strength based on the averaging over many events [8,9,31–33], thus, due to the mirror symmetry of the collision geometry, only the y component of the magnetic field remains sizable, $e\langle B_y\rangle \sim m_\pi^2$, while other components are $\langle B_x\rangle = \langle B_z\rangle = 0$. Hereafter, we use the angle bracket to denote event average. We choose the z axis along the beam direction of the projectile, x axis along the impact parameter b from the target to the projectile, and y axis perpendicular to the reaction plane, as illustrated in Fig. 1.

However, in many cases, the final hadronic signals are measured on the event-by-event basis. Thus, it is important to study how the magnetic fields are generated on the event-by-event basis. Such a study was recently initiated by Bzdak and Skokov [34]. They showed that the x component of the magnetic field can be as strong as the y component on the event-by-event basis, due to the fluctuation of the proton positions in the colliding nuclei. Besides, they also found that the event-by-event generated electric field can be comparable to the magnetic field.

The aim of our work is to give a detailed study of the space-time structure of the event-by-event generated electromagnetic fields in the heavy-ion collisions. We perform our calculation by using the heavy ion jet interaction generator (HIJING) model [35–37]. HIJING is a Monte Carlo event generator for hadron productions in high energy p + p, p + A, and A + A collisions. It is essentially a two-component model, which describes the production of hard parton jets and the soft interaction between nucleon remnants. In HIJING, the hard jet production is controlled by perturbative QCD, and the

*deng@fias.uni-frankfurt.de
†xhuang@itp.uni-frankfurt.de

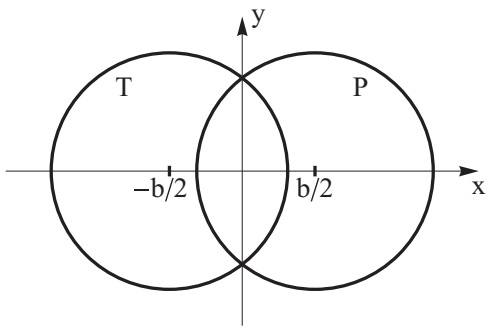

FIG. 1. The geometrical illustration of the off-central collisions with impact parameter b. Here "T" for target and "P" for projectile.

interaction of nucleon remnants via soft gluon exchanges is described by the string model [38].

This paper is organized as follows. We give a general setup of our calculation in Sec. II. In Sec. III, we present our numerical results. We discuss the influence of the nontrivial electromagnetic response of the QGP on the time evolution of the electromagnetic fields in Sec. IV. We conclude with discussions and summary in Sec. V. We use natural unit $\hbar = c = 1$.

II. GENERAL SETUP

We use the Liénard-Wiechert potentials to calculate the electric and magnetic fields at a position $\mathbf{r}$ and time t,

$$e\mathbf{E}(t,\mathbf{r}) = \frac{e^2}{4\pi}\sum_n Z_n \frac{\mathbf{R}_n - R_n\mathbf{v}_n}{(R_n - \mathbf{R}_n\cdot\mathbf{v}_n)^3}\left(1-v_n^2\right), \quad (2.1)$$

$$e\mathbf{B}(t,\mathbf{r}) = \frac{e^2}{4\pi}\sum_n Z_n \frac{\mathbf{v}_n\times\mathbf{R}_n}{(R_n - \mathbf{R}_n\cdot\mathbf{v}_n)^3}\left(1-v_n^2\right), \quad (2.2)$$

where Z_n is the charge number of the nth particle, $\mathbf{R}_n = \mathbf{r} - \mathbf{r}_n$ is the relative position of the field point $\mathbf{r}$ to the source point $\mathbf{r}_n$, and $\mathbf{r}_n$ is the location of the nth particle with velocity $\mathbf{v}_n$ at the retarded time $t_n = t - |\mathbf{r} - \mathbf{r}_n|$. The summations run over all charged particles in the system. Although there are singularities at $R_n = 0$ in Eqs. (2.1)–(2.2), in practical calculation of $\mathbf{E}$ and $\mathbf{B}$ at given $(t,\mathbf{r})$, the events causing such singularities rarely appear. So, we omit such events in our numerical code. In the nonrelativistic limit, $v_n \ll 1$, Eq. (2.1) reduces to the Coulomb's law and Eq. (2.2) reduces to the Biot-Savart law for a set of moving charges,

$$e\mathbf{E}(t,\mathbf{r}) = \frac{e^2}{4\pi}\sum_n Z_n \frac{\mathbf{R}_n}{R_n^3}, \quad (2.3)$$

$$e\mathbf{B}(t,\mathbf{r}) = \frac{e^2}{4\pi}\sum_n Z_n \frac{\mathbf{v}_n\times\mathbf{R}_n}{R_n^3}. \quad (2.4)$$

To calculate the electromagnetic fields at moment t, we need to know the full phase-space information of all charged particles before t. In the HIJING model, the position of each nucleon before collision is sampled according to the Woods-Saxon distribution. The energy for each nucleon is set to be $\sqrt{s}/2$ in the center-of-mass frame. Assuming that the nucleons have no transverse momenta before collision, the value of the velocity of each nucleon is given by $v_z^2 = 1 - (2m_N/\sqrt{s})^2$, where m_N is the mass of the nucleon. At RHIC and LHC, v_z is very large, so the nuclei are Lorentz contracted to pancake shapes.

We set the initial time $t = 0$ as the moment when the two nuclei completely overlap. The collision time for each nucleon is given according to its initial longitudinal position $z_N^L = z_N 2m_N/\sqrt{s}$ and velocity v_z, where z_N is the initial longitudinal position of nucleon in the rest frame of the nucleus. The probability of two nucleon colliding at a given impact parameter b is determined by the Glauber model. In this paper, we call nucleons without any interaction spectators, and those that suffer at least once elastic or inelastic collision participants before their first collision. The participants will exchange their momenta and energies and become remnants after collision. Differently from the spectators and the participants, the remnants can have finite transverse momenta. In our calculation, we find that although the spectators and participants are the main sources of fields at $t \leqslant 0$, remnants can give important contributions at $t > 0$. In the HIJING model, we neglect the back reaction of the electromagnetic field on the motions of the the charged particles. This is a good approximation before the collision happens because the electromagnetic field is weak at that time. We will discuss the feed back effect of the electromagnetic fields on QGP in Sec. IV by using a magnetohydrodynamic treatment.

After collision, many partons may be produced and the hot, dense QGP may form. As the QGP is nearly neutral, we neglect the contributions from the produced partons to the generation of the electromagnetic field. However, if the electric conductivity of the QGP is large, the QGP can have significant response to the change of the external electromagnetic field. This can become substantial for the time evolution of the fields in the QGP. We will discuss this point in detail in Sec. IV.

III. NUMERICAL RESULTS

A. Impact parameter dependence

We first show the impact parameter dependence of the electromagnetic fields at $\mathbf{r} = \mathbf{0}$ and $t = 0$. The left panel of Fig. 2 is the results for Au + Au collision at RHIC energy $\sqrt{s} = 200$ GeV; the right panel of Fig. 2 is for Pb Pb collision at LHC energy $\sqrt{s} = 2.76$ TeV. As seen from Eq. (2.2), $\langle B_x(t,\mathbf{0})\rangle = 0$, while $\langle B_y(t,\mathbf{0})\rangle < 0$ when $b > 0$.

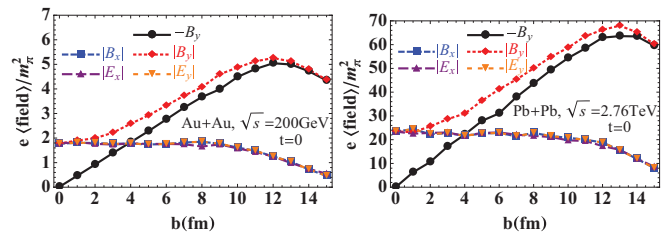

FIG. 2. (Color online) The electromagnetic fields at $t = 0$ and $\mathbf{r} = \mathbf{0}$ as functions of the impact parameter b.

Also, from Eqs. (2.1)–(2.2), we find that there are always $|E_y(0,\mathbf{0})| \approx |B_x(0,\mathbf{0})|$ and $|B_y(0,\mathbf{0})| \geqslant |E_x(0,\mathbf{0})|$ when v_z is large [see Eqs. (3.2)–(3.3)]. These facts are reflected in Fig. 2. Although the x component of the magnetic field as well as the x and y components of the electric field vanish after averaging over many events, their magnitudes in each event can be huge due to the fluctuations of the proton positions in the nuclei. Thus, following Bzdak and Skokov [34], we plot the averaged absolute values $\langle|E_{x,y}|\rangle$ and $\langle|B_{x,y}|\rangle$ at $\mathbf{r} = \mathbf{0}$ and $t = 0$. Similar with the findings in Ref. [34], we find that $\langle|B_x|\rangle$, $\langle|E_x|\rangle$, and $\langle|E_y|\rangle$ are comparable to $\langle|B_y|\rangle$, and the following equalities hold approximately, $\langle|E_x|\rangle \approx \langle|E_y|\rangle \approx \langle|B_x|\rangle$. But our results at RHIC energy are about three times smaller than that obtained in Ref. [34]. We checked that this is because the thickness of the nuclei in our calculation is finite while the authors of Ref. [34] assumed that the nuclei are infinitely thin. We can also observe that, at small b region, contrary to $\langle B_y\rangle$ which is proportional to b, the fields caused by fluctuation are not sensitive to b.

B. Collision energy dependence

We see from Fig. 2 that the magnitudes of all the fields at LHC energy is around 14 times bigger than that at RHIC energy. To study the collision energy dependence more carefully, we calculate the fields at $t = 0$ and $\mathbf{r} = \mathbf{0}$ for different $\sqrt{s}$. To high precision, the linear dependence of the fields on the collision energy is obtained, as shown in Fig. 3. Thus, the following scaling law holds for event-by-event generated electromagnetic fields as well as for event-averaged magnetic fields,

$$e\text{Field} \propto \sqrt{s} f(b/R_A), \tag{3.1}$$

where R_A is the radius of the nucleus and $f(b/R_A)$ is a universal function, which has the shapes as shown in Fig. 2 for $\langle|B_{x,y}|\rangle$, $\langle|E_{x,y}|\rangle$, and $\langle B_y\rangle$.

Actually, a more general form of Eq. (3.1) can be derived from Eqs. (2.1)–(2.2). As the fields at $t = 0$ are mainly caused by spectators and participants whose velocity $v_n = v_z = \sqrt{1-(2m_N/\sqrt{s})^2} \approx 1$, the electric and magnetic fields

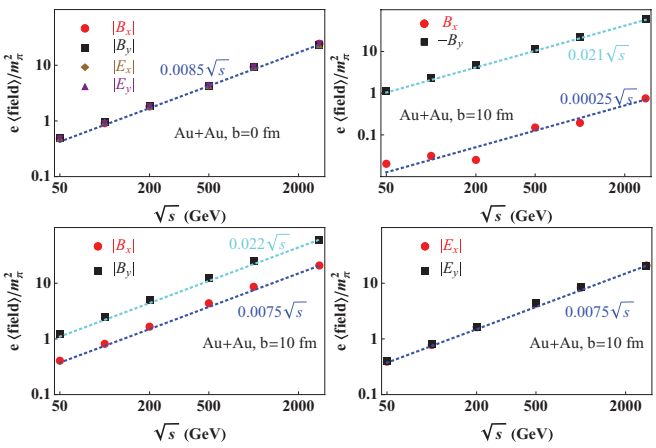

FIG. 3. (Color online) The collision energy dependence of the electromagnetic fields at $\mathbf{r} = \mathbf{0}$ and $t = 0$.

at $t = 0$ in the transverse plane can be expressed as

$$e\mathbf{E}_\perp(0,\mathbf{r}) \approx \frac{e^2}{4\pi}\frac{\sqrt{s}}{2m_N}\sum_n \frac{\mathbf{R}_{n\perp}}{R_{n\perp}^3}, \tag{3.2}$$

$$e\mathbf{B}_\perp(0,\mathbf{r}) \approx \frac{e^2}{4\pi}\frac{\sqrt{s}}{2m_N}\sum_n \frac{\mathbf{e}_{nz}\times\mathbf{R}_{n\perp}}{R_{n\perp}^3}, \tag{3.3}$$

where $\mathbf{e}_{nz}$ is the unit vector in $\pm z$ direction depending on whether the nth proton is in the target or in the projectile, $\mathbf{R}_{n\perp}$ is the transverse position of the nth proton, which is independent of $\sqrt{s}$, and $R_{n\perp} = |\mathbf{R}_{n\perp}|$.

C. Spatial distribution

The spatial distributions of the magnetic and electric fields are evidently inhomogeneous. We show in Fig. 4 the contour plots of $\langle B_{x,y,z}\rangle$, $\langle E_{x,y,z}\rangle$, $\langle|B_{x,y,z}|\rangle$, and $\langle|E_{x,y,z}|\rangle$ at $t = 0$ in the transverse plane at RHIC energy. The upper two panels are for $b = 0$ and the lower two panels are for $b = 10$ fm. The spatial distribution of the transverse fields for LHC energy is merely the same as Fig. 4 but the fields have $2760/200 \approx 14$ times larger magnitudes everywhere according to Eqs. (3.2)–(3.3). The spatial distribution of the fields in the reaction plane was studied in Ref. [32].

First, as we expected, the longitudinal fields $\langle B_z\rangle$, $\langle E_z\rangle$, $\langle|B_z|\rangle$, and $\langle|E_z|\rangle$ are much smaller than the transverse fields. Second, the event-averaged fields $\langle B_{x,y}\rangle$ and $\langle E_{x,y}\rangle$ distribute similarly with the fields generated by two uniformly charged, oppositely moving, discs. Third, the spatial distribution of the magnetic fields is very different from that of the electric fields on the event-by-event basis. For central collisions, both $\langle|B_x|\rangle$ and $\langle|B_y|\rangle$ distribute circularly and concentrate at $\mathbf{r} = \mathbf{0}$, while $\langle|E_x|\rangle$ and $\langle|E_y|\rangle$ peak around $x = \pm R_A$ and $y = \pm R_A$ with R_A the radius of the nucleus. We notice that for off-central collisions, the y component of the electric field varies steeply along y direction, reflecting the fact that at $t = 0$ a large amount of net charge stays temporally in the almond-shaped overlapping region.

D. Probability distribution over events

Although we used the event-averaged absolute values $\langle|B_{x,y}|\rangle$ and $\langle|E_{x,y}|\rangle$ to characterize the event-by-event fluctuations of the electromagnetic fields, it would have more practical relevance to see the probability distribution of the magnetic field, defined as

$$P(B_x, B_y) \equiv \frac{1}{N}\frac{d^2N}{dB_x dB_y}, \tag{3.4}$$

where N is the number of events. Similarly, we can define $P(E_x, E_y)$. After simulating 10^6 events, we obtain $P(B_x, B_y)$ and $P(E_x, E_y)$ at $t = 0$ and $\mathbf{r} = \mathbf{0}$ for Au + Au collisions at $\sqrt{s} = 200$ GeV, as shown in Fig. 5. As expected, the probability distribution of the magnetic (electric) field peaks at $\mathbf{B} = \mathbf{0}$ ($\mathbf{E} = \mathbf{0}$) for central collisions, while the probability distribution for magnetic field is shifted to finite B_y for off-central collisions. This is more clearly shown in Fig. 6, where we depict the one-dimensional probability density $P(B_x) \equiv$

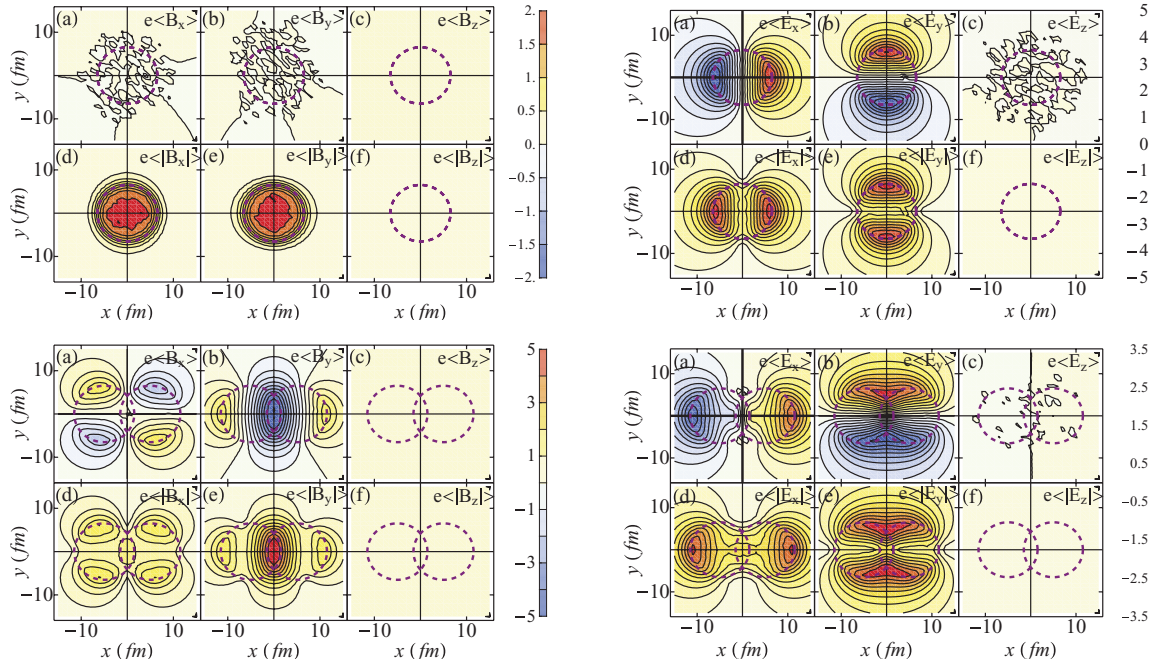

FIG. 4. (Color online) The spatial distributions of the electromagnetic fields in the transverse plane at $t = 0$ for $b = 0$ (upper panels) and $b = 10$ fm (lower panels) at RHIC energy. The unit is m_π^2. The dashed circles indicate the two colliding nuclei.

$\int dB_y P(B_x, B_y)$ (other probability densities are analogously defined).

The probability distributions for Pb + Pb collisions at $\sqrt{s} = 2.76$ TeV have analogous shapes with Fig. 5 but much more spread, as clearly shown in the lower panels of Fig. 6. This is because the strength of the field generated at LHC can be obtained approximately from that at RHIC by a $\sqrt{s_{\rm LHC}/s_{\rm RHIC}}$ scaling according to Eqs. (3.2)–(3.3). Thus, after normalization, the probability distributions at LHC energy are related to that at RHIC energy by

$$P_{\rm LHC}(B_x, B_y) \approx \frac{s_{\rm RHIC}}{s_{\rm LHC}} P_{\rm RHIC}\left(\sqrt{\frac{s_{\rm RHIC}}{s_{\rm LHC}}} B_x, \sqrt{\frac{s_{\rm RHIC}}{s_{\rm LHC}}} B_y\right), \tag{3.5}$$

$$P_{\rm LHC}(E_x, E_y) \approx \frac{s_{\rm RHIC}}{s_{\rm LHC}} P_{\rm RHIC}\left(\sqrt{\frac{s_{\rm RHIC}}{s_{\rm LHC}}} E_x, \sqrt{\frac{s_{\rm RHIC}}{s_{\rm LHC}}} E_y\right). \tag{3.6}$$

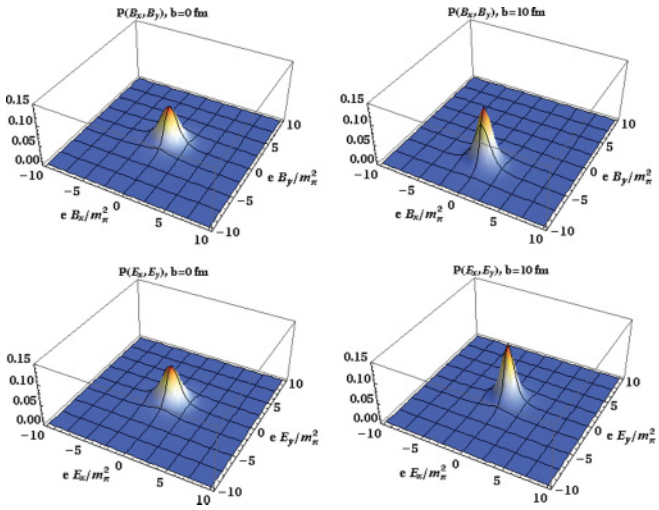

FIG. 5. (Color online) The probability densities $P(B_x, B_y)$ and $P(E_x, E_y)$ for different impact parameters for Au + Au collisions at $\sqrt{s} = 200$ GeV.

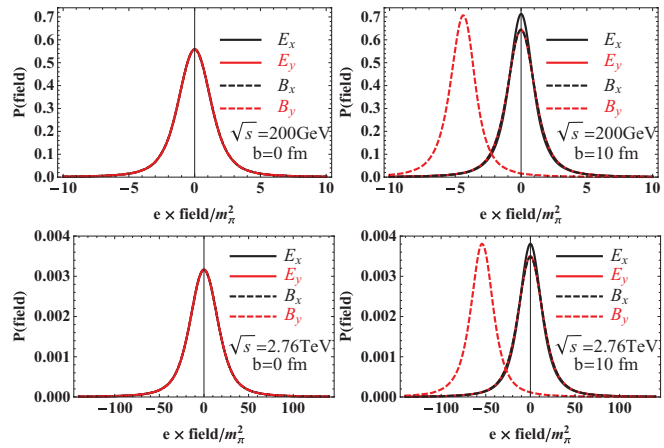

FIG. 6. (Color online) The probability densities $P(B_{x,y})$ and $P(E_{x,y})$ for central collisions $b = 0$ and off-central collisions $b = 10$ fm for Au + Au collisions (upper panels) at $\sqrt{s} = 200$ GeV and for Pb Pb collisions at $\sqrt{s} = 2.76$ TeV (lower panels).

E. Early-stage time evolution

In Fig. 7, we show our results of the early-stage time evolution of the electromagnetic fields at $\mathbf{r} = \mathbf{0}$ in both central collisions and off-central collisions with $b = 10$ fm, for Au + Au collisions at $\sqrt{s} = 200$ GeV and for Pb + Pb collision at $\sqrt{s} = 2.76$ TeV. We take into account the contributions from charged particles in spectators, participants, and remnants. Around $t = 0$, we checked that the contributions from the remnants are negligibly small, while the contributions from participants can be as large as that from spectators. However, at a later time when the spectators have already moved far away from the collision region, the contributions from the remnants become important because they move much slower than the spectators. These remnants can essentially slow down the decay of the transverse fields, as seen from Fig. 7. Another evident effect of the remnants is the substantial enhancements of the longitudinal magnetic and electric fields caused by the position fluctuation of the remnants, which have nonzero transverse momenta. Particularly, although $\langle|B_z|\rangle$ is at least one order smaller than $\langle|B_{x,y}|\rangle$ for $t \lesssim 1$ fm/c, $\langle|E_z|\rangle$ can evolve to the same amount of $\langle|E_{x,y}|\rangle$ in a very short time after collision and then they decay very slowly.

For central collisions, all the fields are generated due to the position fluctuations of the charged particles. As seen from Fig. 7, these fluctuations lead to sizable $\langle|E_x|\rangle = \langle|E_y|\rangle$ and $\langle|B_x|\rangle = \langle|B_y|\rangle$ around $t = 0$, but they drop very fast. Note that the fields drop faster for larger collision energy $\sqrt{s}$.

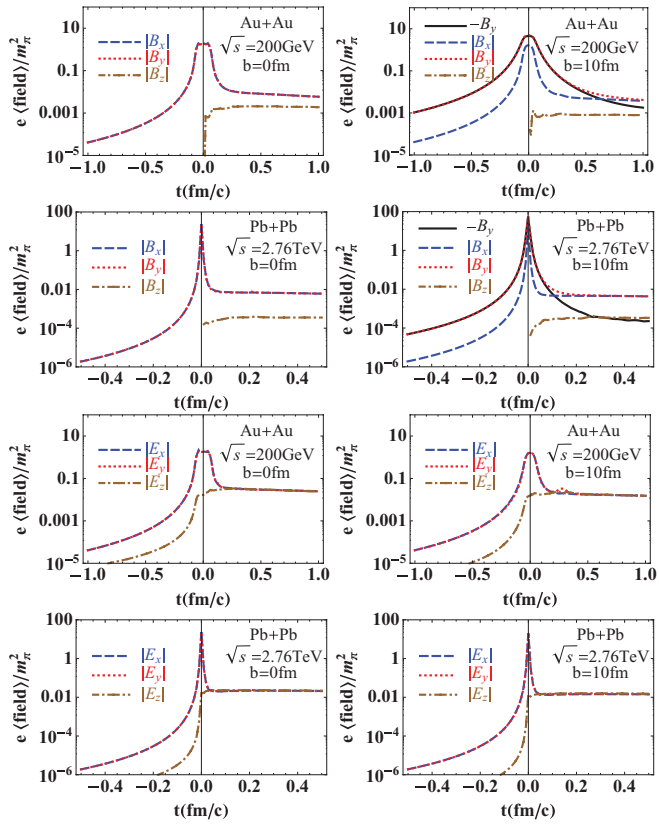

FIG. 7. (Color online) The time evolution of electromagnetic fields at $\mathbf{r} = 0$ with impact parameter $b = 0$, and $b = 10$ for Au + Au collisions at $\sqrt{s} = 200$ GeV and Pb + Pb collisions at $\sqrt{s} = 2.76$ TeV. After collision, the remnants can essentially slow down the decay of the transverse fields, and enhance the longitudinal fields.

For off-central collisions, the y component of the magnetic field are much larger than other fields at $t = 0$. But at a later time when the spectators move far away, the contributions of remnants dominate, and lead to $\langle|B_y|\rangle \approx \langle|B_x|\rangle > \langle B_y\rangle$.

A common feature of all the fluctuation-caused transverse fields is that they all increase very fast before collision (due to the fast approaching of the nuclei), then they drop steeply after $t = 0$ (due to the high-speed leaving of the spectators away from the collision center), and then decay very slowly (due to that contribution from the slowly moving remnants take over that from the spectators). After the early-stage evolution, the produced QGP may get enough time to respond to the electromagnetic fields, which may substantially modify the picture of evolution. We discuss this point in the next section.

IV. RESPONSE OF THE QUARK-GLUON PLASMA TO ELECTROMAGNETIC FIELDS

In the calculations above, we have neglected the electromagnetic response of the matter produced in the collision (i.e., we assumed the produced matter is ideally electrically insulating). However, if the produced matter, after a short early-stage evolution, is in the QGP phase, the electric conductivity σ is not negligible. At high temperature, the perturbative QCD gives that $\sigma \approx 6T/e^2$ [39], and the lattice calculations give that $\sigma \approx 7C_{\rm EM}T$ [40], or $\sigma \approx 0.4C_{\rm EM}T$ [41,42], or $\sigma \approx (1/3)C_{\rm EM}T - C_{\rm EM}T$ [42,43] for temperature of several T_c, where $C_{\rm EM} \equiv \sum_f e_f^2$, $f = u, d, s$, and e_f is the charge of quark with flavor f. Thus it is expected that the QGP can have nontrivial electromagnetic response. Such electromagnetic response can substantially influence the time evolution of the electromagnetic fields in the QGP.

To have an estimation of the electromagnetic response of QGP, we use the following Maxwell's equations,

$$\nabla \times \mathbf{E} = -\frac{\partial \mathbf{B}}{\partial t}, \tag{4.1}$$

$$\frac{1}{\mu}\nabla \times \mathbf{B} = \epsilon\frac{\partial \mathbf{E}}{\partial t} + \mathbf{J}, \tag{4.2}$$

where μ and ϵ are the permeability and permittivity of the QGP, respectively, and are assumed as constants. $\mathbf{J}$ is the electric current determined by the Ohm's law,

$$\mathbf{J} = \sigma\left(\mathbf{E} + \mathbf{v} \times \mathbf{B}\right), \tag{4.3}$$

where $\mathbf{v}$ is the flow velocity of QGP. Using Eq. (4.3), we can rewrite the Maxwell's equations as

$$\frac{\partial \mathbf{B}}{\partial t} = \nabla \times (\mathbf{v} \times \mathbf{B}) + \frac{1}{\sigma\mu}\left(\nabla^2\mathbf{B} - \mu\epsilon\frac{\partial^2 \mathbf{B}}{\partial t^2}\right), \tag{4.4}$$

$$\frac{\partial \mathbf{E}}{\partial t} + \frac{\partial \mathbf{v}}{\partial t} \times \mathbf{B} = \mathbf{v} \times (\nabla \times \mathbf{E}) + \frac{1}{\sigma\mu}\left(\nabla^2\mathbf{E} - \mu\epsilon\frac{\partial^2 \mathbf{E}}{\partial t^2}\right), \tag{4.5}$$

where we have used the Gauss's laws $\nabla \cdot \mathbf{B} = 0$ and $\nabla \cdot \mathbf{E} = \rho = 0$ with the assumption that the net electric charge density of the QGP is zero. Equation (4.4) is the induction equation, which plays a central role in describing the dynamo mechanism of stellar magnetic field generation. The first terms on the right-hand sides of Eqs. (4.4)–(4.5) are the convection terms, while the last terms are the diffusion terms. The ratio of these two types of terms are characterized by the magnetic Reynolds number R_m,

$$R_m \equiv LU\sigma\mu, \tag{4.6}$$

where L is the characteristic length or time scale of the QGP, U is the characteristic velocity of the flow.

Because the theoretical result of σ is quite uncertain, the value of R_m is also uncertain. For example, by assuming $\mu = \epsilon = 1$, setting the characteristic length scale $L \sim 10$ fm, and the typical velocity $U \sim 0.5$, we can estimate R_m at $T = 350$ MeV as $R_m \sim 0.2$ if we use $\sigma \approx 0.4 C_{\rm EM} T$ in Refs. [41,42], or $R_m \sim 4$ if we use $\sigma \approx 7 C_{\rm EM} T$ in Ref. [40], or $R_m \sim 600$ if we use $\sigma \approx 6T/e^2$ in Ref. [39].

If $R_m \ll 1$, we can neglect the convection terms in Eq. (4.4) and Eq. (4.5). Tuchin studied this case [27] (with additional condition $U \ll 1$ so that the second-order time-derivative terms in the diffusion terms are neglected), and concluded that the magnetic field can be considered as approximately stationary during the QGP lifetime.[1]

If $R_m \gg 1$, we can neglect the diffusion terms in Eqs. (4.4)–(4.5), i.e., take the ideally conducting limit,

$$\frac{\partial \mathbf{B}}{\partial t} = \nabla \times (\mathbf{v} \times \mathbf{B}), \tag{4.7}$$

$$\mathbf{E} = -\mathbf{v} \times \mathbf{B}. \tag{4.8}$$

It is well known that Eq. (4.7) leads to the frozen-in theorem for ideally conducting plasma (i.e., the magnetic lines are frozen in the plasma elements or more precisely the magnetic flux through a closed loop defined by plasma elements keeps constant [44]).

We now use Eqs. (4.7)–(4.8) to estimate how the electromagnetic field evolves in a QGP with $R_m \gg 1$. To this purpose, we have to know the evolution of $\mathbf{v}$ first. By assuming that the bulk evolution of the QGP is governed by strong dynamics, we can neglect the influence of the electromagnetic field on the evolution of the velocity $\mathbf{v}$. We assume the Bjorken picture for the longitudinal expansion,

$$v_z = \frac{z}{t}. \tag{4.9}$$

[1]To reach this conclusion, Tuchin used $\sigma = 6T^2/T_c$ to estimate the magnetic diffusion time $\tau = (L/2)^2\sigma/4$ and found that, for $L = 10$ fm and $T = 2T_c \approx 400$MeV, $\tau \approx 150$ fm is much longer than the lifetime of the QGP. However, if, for example, $\sigma \approx 0.4 C_{\rm EM} T$ is used, the magnetic diffusion time is $\tau \approx 0.3$ fm, which is much shorter than what Tuchin obtained.

Because the early transverse expansion is slow, following Ref. [45], we adopt a linearized ideal hydrodynamic equation to describe the transverse flow velocity $\mathbf{v}_\perp$,

$$\frac{\partial}{\partial t}\mathbf{v}_\perp = -\frac{1}{\varepsilon + P}\nabla_\perp P = -c_s^2 \nabla_\perp \ln \mathfrak{s}, \tag{4.10}$$

where we used $\varepsilon + P = T\mathfrak{s}$, $\mathfrak{s}$ is the entropy density, and $c_s = \sqrt{\partial P/\partial \varepsilon}$ is the speed of sound. For simplicity, we choose an initial Gaussian transverse entropy density profile as in [45],

$$\mathfrak{s}(x, y) = \mathfrak{s}_0 \exp\left(-\frac{x^2}{2a_x^2} - \frac{y^2}{2a_y^2}\right), \tag{4.11}$$

where $a_{x,y}$ are the root-mean-square widths of the transverse distribution. They are of order of the nuclei radii if the impact parameter is not large. For example, for Au + Au collisions at RHIC, $a_x \sim a_y \sim 3$ fm for $b = 0$, and $a_x \sim 2$ fm, $a_y \sim 3$ fm for $b = 10$ fm. One can then easily solve Eq. (4.10) and obtain,

$$v_x = \frac{c_s^2}{a_x^2} xt, \tag{4.12}$$

$$v_y = \frac{c_s^2}{a_y^2} yt. \tag{4.13}$$

Substituting the velocity fields above into Eq. (4.7), we obtain a linear differential equation for $\mathbf{B}(t)$. For a given initial condition $\mathbf{B}^0(\mathbf{r}) = \mathbf{B}(t = t_0, \mathbf{r})$ where t_0 is the formation time of the QGP, it can be solved analytically,

$$B_x(t, x, y, z) = \frac{t_0}{t} e^{-\frac{c_s^2}{2a_y^2}(t^2 - t_0^2)} \times B_x^0\left(x e^{-\frac{c_s^2}{2a_x^2}(t^2 - t_0^2)}, y e^{-\frac{c_s^2}{2a_y^2}(t^2 - t_0^2)}, z\frac{t_0}{t}\right), \tag{4.14}$$

$$B_y(t, x, y, z) = \frac{t_0}{t} e^{-\frac{c_s^2}{2a_x^2}(t^2 - t_0^2)} \times B_y^0\left(x e^{-\frac{c_s^2}{2a_x^2}(t^2 - t_0^2)}, y e^{-\frac{c_s^2}{2a_y^2}(t^2 - t_0^2)}, z\frac{t_0}{t}\right). \tag{4.15}$$

Because B_z is always much smaller than B_x and B_y, we are not interested in it. The electric fields can be obtained from Eq. (4.8) once we have $\mathbf{B}(t, \mathbf{r})$.

To reveal the physical content in Eqs. (4.14)–(4.15), we notice that, by integrating Eq. (4.9), Eq. (4.12), and Eq. (4.13), a fluid cell located at (x_0, y_0, z_0) at time t_0 will flow to the coordinate (x, y, z) at time t with

$$x = x_0 \exp\left[\frac{c_s^2}{2a_x^2}\left(t^2 - t_0^2\right)\right], \tag{4.16}$$

$$y = y_0 \exp\left[\frac{c_s^2}{2a_y^2}\left(t^2 - t_0^2\right)\right], \tag{4.17}$$

$$z = z_0 \frac{t}{t_0}. \tag{4.18}$$

Thus, we can rewrite Eqs. (4.14)–(4.15) as

$$B_x(t,x,y,z) = \frac{t_0}{t} e^{-\frac{c_s^2}{2a_y^2}(t^2-t_0^2)} B_x(t_0,x_0,y_0,z_0), \quad (4.19)$$

$$B_y(t,x,y,z) = \frac{t_0}{t} e^{-\frac{c_s^2}{2a_x^2}(t^2-t_0^2)} B_y(t_0,x_0,y_0,z_0). \quad (4.20)$$

As the areas of the cross sections of the QGP expand according to $t\exp(\frac{c_s^2}{2a_y^2}t^2)$ in the y-z plane and $t\exp(\frac{c_s^2}{2a_x^2}t^2)$ in the x-z plane, Eqs. (4.19)–(4.20) mean that the magnetic line flows with the fluid cell and is diluted due to the expansion of the QGP. These are just the manifestations of the frozen-in theorem. We also note that Eqs. (4.14)–(4.15) can be written in explicit scaling forms,

$$t\, e^{\frac{c_s^2}{2a_y^2}t^2} B_x\left(t, x e^{\frac{c_s^2}{2a_x^2}t^2}, y e^{\frac{c_s^2}{2a_y^2}t^2}, z\, t\right) = t_0\, e^{\frac{c_s^2}{2a_y^2}t_0^2} B_x\left(t_0, x e^{\frac{c_s^2}{2a_x^2}t_0^2}, y e^{\frac{c_s^2}{2a_y^2}t_0^2}, z\, t_0\right), \quad (4.21)$$

$$t\, e^{\frac{c_s^2}{2a_x^2}t^2} B_y\left(t, x e^{\frac{c_s^2}{2a_x^2}t^2}, y e^{\frac{c_s^2}{2a_y^2}t^2}, z\, t\right) = t_0\, e^{\frac{c_s^2}{2a_x^2}t_0^2} B_y\left(t_0, x e^{\frac{c_s^2}{2a_x^2}t_0^2}, y e^{\frac{c_s^2}{2a_y^2}t_0^2}, z\, t_0\right). \quad (4.22)$$

From Eqs. (4.14)–(4.15), we see that the evolution of $\mathbf{B}$ is strongly influenced by its initial spatial distribution. However, the time evolution of the magnetic fields at the center of the collision region, $\mathbf{r} = \mathbf{0}$, takes very simple forms,

$$B_x(t,\mathbf{0}) = \frac{t_0}{t} e^{-\frac{c_s^2}{2a_y^2}(t^2-t_0^2)} B_x^0(\mathbf{0}), \quad (4.23)$$

$$B_y(t,\mathbf{0}) = \frac{t_0}{t} e^{-\frac{c_s^2}{2a_x^2}(t^2-t_0^2)} B_y^0(\mathbf{0}). \quad (4.24)$$

Setting $a_x \sim a_y \sim 3$ fm and $c_s^2 \sim 1/3$, we see from Eqs. (4.23)–(4.24) that for $t \lesssim 5$ fm the magnetic fields decay inversely proportional to time.

V. CONCLUSION

In summary, we have utilized the HIJING model to investigate the generation and evolution of the electromagnetic fields in heavy-ion collisions. The cases of Au + Au collisions at $\sqrt{s} = 200$ GeV and Pb Pb collisions at $\sqrt{s} = 2.76$ TeV are considered in detail. Although after averaging over many events only the component B_y remains, the event-by-event fluctuation of the positions of charged particles can induce components B_x, E_x, E_y as large as B_y. They can reach the order of several m_π^2/e. The spatial structure of the electromagnetic field is studied and a very inhomogeneous distribution is found. We study also the time evolution of the fields including the early-stage and the QGP-stage evolutions. We find that the remnants can give substantial contribution to the fields during the early-stage evolutions. The nontrivial electromagnetic response of the QGP, which is sensitive to the electric conductivity, gives nontrivial time dependence of the fields in it (see Sec. IV). We check both in numerical calculation (Fig. 3) and analytical derivations [Eqs. (3.2)–(3.3)] that the electric and magnetic fields at $t = 0$ have approximately linear dependence on the collision energy $\sqrt{s}$.

The strong event-by-event fluctuation of the electromagnetic field may lead to important implications for observables that are sensitive to the electromagnetic field. We point out two examples here.

(i) From Fig. 2 we see that although the electric fields E_x and E_y at $\mathbf{r} = \mathbf{0}$ can be very strong, they are roughly equal. Then one expects that the strong electric fields should not have a significant contribution for the correlation observable $\langle\cos(\phi_1 + \phi_2 - 2\Psi_{RP})\rangle$, which is sensitive to the chiral magnetic effect [46], where $\phi_{1,2}$ are the azimuthal angles of the final-state charged particles, and Ψ_{RP} is the azimuthal angle of the reaction plane. On the other hand, from Fig. 4 we see that in the overlapping region for peripheral collisions, the electric field perpendicular to the reaction plane has a larger gradient than that parallel to the reaction plane. Thus, a strong, out-of-plane electric field develops away from the origin $\mathbf{r} = \mathbf{0}$ in the overlapping region. Note that the direction of this electric field points outside of the reaction plane. If the electric conductivity of the matter produced in the collision is large, this out-of-plane electric field can drive positive (negative) charges to move outward (toward) the reaction plane, and thus induce an electric quadrupole moment. Such an electric quadrupole moment, as argued in Ref. [30], can lead to an elliptic flow imbalance between π^+ and π^-. Thus, it will be interesting to study how strong the electric quadrupole moment induced by this out-of-plane electric field can be. Note that such electric quardrupole configuration does not contribute to the correlation $\langle\cos(\phi_1 + \phi_2 - 2\Psi_{RP})\rangle$.

(ii) It is known that quarks produced in off-central heavy-ion collision can be possibly polarized due to the spin-orbital coupling of QCD [47–49]. The strong magnetic field can cause significant polarization of quarks as well through the interaction between the quark magnetic moment and the magnetic field. As estimated by Tuchin [27], a magnetic field of order m_π^2/e can almost immediately polarize light quarks. Such polarization, contrary to the polarization due to spin-orbital coupling, will depend on the charges of quarks, and build a spin-charge correlation for quarks (i.e., the positively charged quarks are polarized along the magnetic field while the negatively charged quarks are polarized opposite to the magnetic field). If we expect that the strong interaction in the QGP and the hadronization processes do not wash out this spin-charge correlations, we should observe similar spin-charge correlation for final-state charged hadrons.

ACKNOWLEDGMENTS

We thank A. Bzdak, V. Skokov, H. Warringa, and Z. Xu for helpful discussions and comments. This work was supported by the Helmholtz International Center for FAIR within the framework of the LOEWE program (Landesoffensive zur Entwicklung Wissenschaftlich-Ökonomischer Exzellenz) launched by the State of Hesse. The calculations were partly performed at the Center for Scientific Computing of J. W. Goethe University. Some of the figures were plotted using LevelScheme toolkit [50] for MATHEMATICA.

[1] M. Luzum and P. Romatschke, Phys. Rev. C **78**, 034915 (2008); **79**, 039903(E) (2009).
[2] H. Song, S. A. Bass, U. Heinz, T. Hirano, and C. Shen, Phys. Rev. Lett. **106**, 192301 (2011).
[3] X. N. Wang, Phys. Lett. B **595**, 165 (2004).
[4] I. Vitev and M. Gyulassy, Phys. Rev. Lett. **89**, 252301 (2002).
[5] K. J. Eskola, H. Honkanen, C. A. Salgado, and U. A. Wiedemann, Nucl. Phys. A **747**, 511 (2005).
[6] S. Turbide, C. Gale, S. Jeon, and G. D. Moore, Phys. Rev. C **72**, 014906 (2005).
[7] J. Rafelski and B. Muller, Phys. Rev. Lett. **36**, 517 (1976).
[8] D. E. Kharzeev, L. D. McLerran, and H. J. Warringa, Nucl. Phys. A **803**, 227 (2008).
[9] V. Skokov, A. Y. Illarionov, and V. Toneev, Int. J. Mod. Phys. A **24**, 5925 (2009).
[10] K. Fukushima, D. E. Kharzeev, and H. J. Warringa, Phys. Rev. D **78**, 074033 (2008).
[11] D. E. Kharzeev, Ann. Phys. (NY) **325**, 205 (2010).
[12] STAR Collaboration, B. I. Abelev *et al.*, Phys. Rev. C **81**, 054908 (2010).
[13] STAR Collaboration, B. I. Abelev *et al.*, Phys. Rev. Lett. **103**, 251601 (2009).
[14] N. N. Ajitanand, R. A. Lacey, A. Taranenko, and J. M. Alexander, Phys. Rev. C **83**, 011901 (2011).
[15] P. Christakoglou, J. Phys. G **38**, 124165 (2011).
[16] S. Pratt, S. Schlichting, and S. Gavin, Phys. Rev. C **84**, 024909 (2011).
[17] A. Bzdak, V. Koch, and J. Liao, Phys. Rev. C **81**, 031901 (2010).
[18] A. Bzdak, V. Koch, and J. Liao, Phys. Rev. C **83**, 014905 (2011).
[19] G. L. Ma and B. Zhang, Phys. Lett. B **700**, 39 (2011).
[20] F. Wang, Phys. Rev. C **81**, 064902 (2010).
[21] V. P. Gusynin, V. A. Miransky and I. A. Shovkovy, Phys. Rev. Lett. **73**, 3499 (1994); **76**, 1005(E) (1996).
[22] A. J. Mizher, M. N. Chernodub, and E. S. Fraga, Phys. Rev. D **82**, 105016 (2010).
[23] M. N. Chernodub, Phys. Rev. D **82**, 085011 (2010).
[24] M. N. Chernodub, Phys. Rev. Lett. **106**, 142003 (2011).
[25] R. K. Mohapatra, P. S. Saumia, and A. M. Srivastava, Mod. Phys. Lett. A **26**, 2477 (2011).
[26] K. Tuchin, J. Phys. G **39**, 025010 (2012).
[27] K. Tuchin, Phys. Rev. C **82**, 034904 (2010); **83**, 039903(E) (2011).
[28] X. G. Huang, M. Huang, D. H. Rischke, and A. Sedrakian, Phys. Rev. D **81**, 045015 (2010).
[29] X. G. Huang, A. Sedrakian, and D. H. Rischke, Ann. Phys. (NY) **326**, 3075 (2011).
[30] Y. Burnier, D. E. Kharzeev, J. Liao, and H. U. Yee, Phys. Rev. Lett. **107**, 052303 (2011).
[31] M. Asakawa, A. Majumder, and B. Muller, Phys. Rev. C **81**, 064912 (2010).
[32] V. Voronyuk, V. D. Toneev, W. Cassing, E. L. Bratkovskaya, V. P. Konchakovski, and S. A. Voloshin, Phys. Rev. C **83**, 054911 (2011).
[33] L. Ou and B. A. Li, Phys. Rev. C **84**, 064605 (2011).
[34] A. Bzdak and V. Skokov, Phys. Lett. **B710**, 171 (2012).
[35] X. N. Wang and M. Gyulassy, Phys. Rev. D **44**, 3501 (1991).
[36] W. T. Deng, X. N. Wang, and R. Xu, Phys. Rev. C **83**, 014915 (2011).
[37] W. T. Deng, X. N. Wang, and R. Xu, Phys. Lett. B **701**, 133 (2011).
[38] T. Sjostrand and M. van Zijl, Phys. Rev. D **36**, 2019 (1987).
[39] P. B. Arnold, G. D. Moore, and L. G. Yaffe, J. High Energy Phys. 05 (2003) 051.
[40] S. Gupta, Phys. Lett. B **597**, 57 (2004).
[41] G. Aarts, C. Allton, J. Foley, S. Hands, and S. Kim, Phys. Rev. Lett. **99**, 022002 (2007).
[42] H. T. Ding, A. Francis, O. Kaczmarek, F. Karsch, E. Laermann, and W. Soeldner, Phys. Rev. D **83**, 034504 (2011).
[43] A. Francis and O. Kaczmarek, arXiv:1112.4802 [hep-lat].
[44] J. D. Jackson, *Classical Electrodynamics*, 3rd ed. (Wiley, New York, 1998).
[45] J. Y. Ollitrault, Eur. J. Phys. **29**, 275 (2008).
[46] S. A. Voloshin, Phys. Rev. C **70**, 057901 (2004).
[47] Z. T. Liang and X. N. Wang, Phys. Rev. Lett. **94**, 102301 (2005); **96**, 039901(E) (2006).
[48] J. H. Gao, S. W. Chen, W. t. Deng, Z. T. Liang, Q. Wang, and X. N. Wang, Phys. Rev. C **77**, 044902 (2008).
[49] X. G. Huang, P. Huovinen, and X. N. Wang, Phys. Rev. C **84**, 054910 (2011).
[50] M. A. Caprio, Comput. Phys. Commun. **171**, 107 (2005).